JOURNAL OF MATERIALS SCIENCE 26 (1991) 4648–4656

Influence of fibre weight fraction on failure mechanisms of poly(ethylene terephthalate) reinforced by short-glass-fibres

KIYOSHI TAKAHASHI, NAK-SAM CHOI
Research Institute for Applied Mechanics, Kyushu University, Kasuga-shi, Fukuoka 816, Japan

Failure mechanisms of short-glass-fibre reinforced poly(ethylene terephthalate) were investigated with particular attention to the effects of fibre weight fraction (W_f = 1 wt%, 30 wt% and 60 wt%). A fracture morphology study was carried out for the surface and for the interior of uniaxial tensile specimens. On the surface, tensile cracks occurring mostly at the fibre ends seemed to be more influential in catastrophic fracture initiation with decreasing W_f. However, the failure mechanisms in the interior were different from those on the surface. For specimens of low W_f (1 wt%), shear bands grew around the fibre ends. A "specific layer" was formed in the matrix along the fibre–matrix interface and shear cracks propagated near the interface in the fibre length direction. The fibre pull-out from the matrix as well as the voiding at the fibre ends, induced by the shear cracks, had strong effect on the fracture initiation. For intermediate and higher W_f (30 wt% and 60 wt%), the shear-band induced cracking near the interface caused matrix shear cracking which was the most influential factor in the fracture initiation. The shear failure in the interior almost dominated the fracture processes throughout the specimens.

1. Introduction

Mechanical properties of short-fibre reinforced composites have been extensively investigated in recent years. The properties are much affected by the characteristics of failure processes in fibres, matrix and fibre–matrix interfaces. Failure morphology studies by many authors have shown that the tensile deformation and fracture processes of short-fibre reinforced thermoplastics generally involve microcracking, microvoiding, shear band formation and/or crazing in the matrix and at the interface. Fibre breakage and fibre pull-out are also involved. Those micromechanistic failure processes appear to be associated to some degree with the occurrence of catastrophic fracture initiation. Using notched specimens, Friedrich *et al.* [1–4] and Schultz and Lhymn [5–8] investigated the failure mechanisms in short-fibre reinforced poly(ethylene terephthalate) (PET). Other short-fibre reinforced thermoplastics such as PA [9], PC [3, 10], PES [12, 13], PI [13], PPS [3, 11] and PS [14] were also studied with the notched specimens. Using uniaxial tensile specimens, Sato *et al.* [15, 16] and Curtis *et al.* [18] examined short-fibre/polyamide (PA) 6.6, and Yuan *et al.* [19, 20] studied short-glass-fibre/polyvinyl chloride (PVC). Fractographic observation in these studies, however, has been made mostly on fracture surfaces or unbroken specimen surfaces. As far as the present authors are aware, very little work done to date has been concerned with the morphological difference in micromechanistic fracture processes on and beneath the surface and in the interior of short-fibre reinforced plastics.

In this paper, failure mechanisms of short-glass-fibre reinforced PET were examined on the surface as well as beneath the surface and/or in the interior of specimens under uniaxial tensile loading. The study also considered the effects of fibre weight fraction on the various failure mechanisms which lead to catastrophic fracture initiation.

2. Experimental procedure

2.1. Composites

Dumb-bell-type short-glass-fibre reinforced poly (ethylene terephthalate) (SGFR-PET) tensile specimens were prepared for this study. The commercially available E-glass fibres 10 μm in diameter and 3 mm in length were surface-treated with an epoxy sizing agent and an amino–silane coupling agent. The weight fractions of short-glass-fibres (SGFs) embedded in the PET resin (Mn $\cong 2 \times 10^4$) were 1, 30 and 60 wt %. The pre-compounded pellets were melted in a heated cylinder at 280 °C and were injected into end-gated dumb-bell-shaped moulds at 30 °C by using a conventional screw pre-plasticizing injection moulding machine. The shear rate was about 10^3/sec. The moulded specimen geometry and mould fill direction are shown in Fig. 1. The gauge portion was 70 mm by 12.5 mm with a thickness of 3 mm. Short fibres in the specimens became oriented more to the mould fill direction (X

0022–2461/91 $03.00 + .12

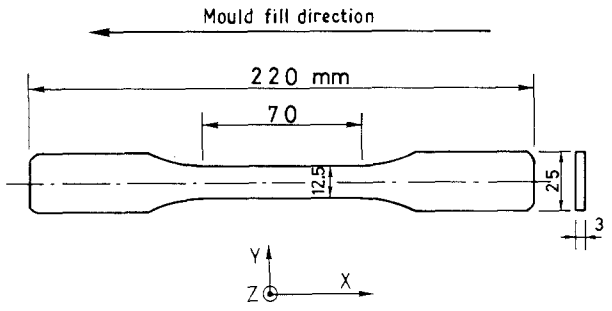

Figure 1 Specimen geometry and mould fill direction.

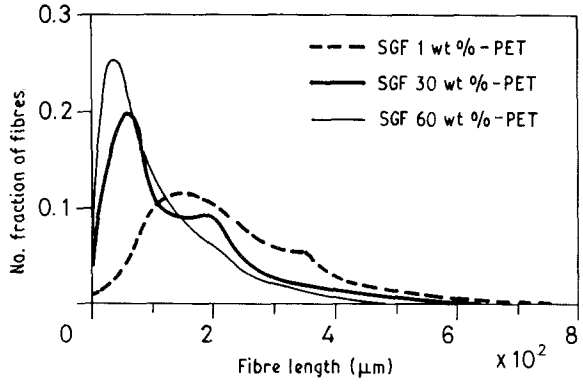

Figure 3 Fibre length distribution in SGFR-PET specimens which depends on fibre weight fraction.

direction) with increasing fibre weight fraction (W_f) as shown in Fig. 2, where X–Z cross sections are presented for the upper half of the specimen thickness (Z direction) t_0. It should be noted that different layers with respect to the thickness direction, i.e., skin and core layers [1–7], were rarely observed. This may be because the specimens were not obtained by machining a larger moulded sheet [1–7] but by direct injection into dumb-bell-shaped moulds. Using dumb-bell-shaped moulds, Bowyer and Bader [22] and Ramsteiner [23] reported similarly that most fibres were aligned along the mould fill direction. Fig. 3 shows fibre length distribution in the specimens with each W_f. Average fibre lengths became shorter as W_f increased: 194 μm for SGF 1 wt %, 123 μm for 30 wt % and 99 μm for 60 wt %. Several studies [24–28] presented similar reduction in fibre length with increasing fibre weight fraction. The fibres may have been severely loaded, bent and then broken by the greater shear forces of the molten matrix when the fibre contents were higher. In contrast to the results, however, other authors [29] obtained no significant decrease in fibre length with the fibre filling level. They explained that it might have been influenced by the various interaction mechanisms of fibre/fibre, fibre/machinery and fibre/matrix. The resin was in a mostly amorphous state. The interfacial coupling state between fibres and matrix was reasonably good.

2.2. Microscopic failure observation

All specimens were uniaxially loaded with a strain rate of 7×10^{-3}/min at a temperature of 23 °C and relative humidity of 55%.

Unreinforced and SGF 1 wt %-PET specimens were unloaded from the loaded state, and were examined under a polarized optical microscope. Failure

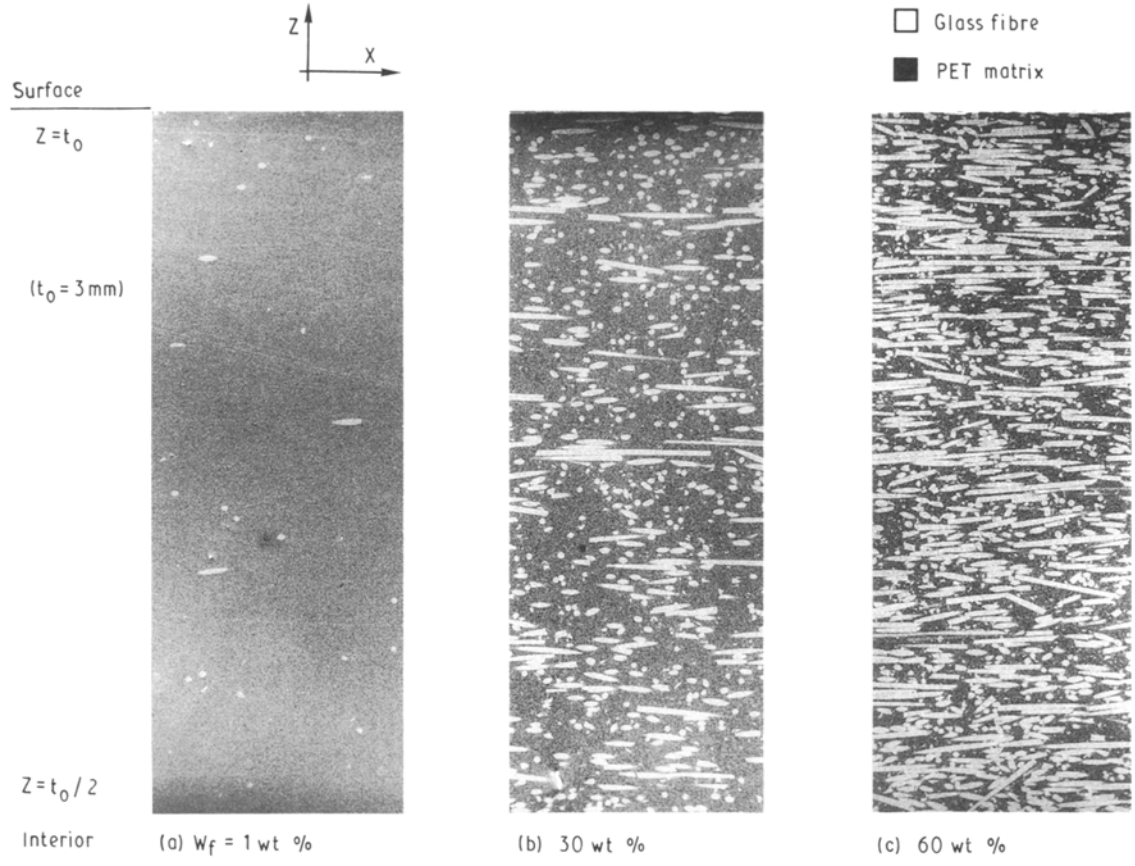

Figure 2 Orientation of short fibres embedded in matrix which depends on fibre weight fraction.

processes were investigated in the interior as well as on the surfaces of the specimens. When it was difficult to observe the processes in the interior from outside because of the occurrence of many micro-failures in the specimen at higher strain, a thinner section was examined. We prepared this section by polishing the deformed gauge portion to a thickness of about 250 μm.

For specimens of SGF 30 wt %-PET and SGF 60 wt %-PET, *in situ* scanning electron microscopic (SEM) observation was carried out, as Sato *et al.* [16] did in order to examine failure mechanisms on the specimen surface. Because the specimens, even before being loaded, were optically not very transparent, the above sectioning method was adopted to study the mechanisms in the interior.

3. Results and discussion

3.1. Stress–strain curves

Fig. 4 shows typical stress–strain curves for SGF 1 wt %, SGF 30 wt % and SGF 60 wt %-PET specimens. With increasing fibre weight fraction, fracture strength and elastic modulus of the specimens became greater, while the fracture strain became less. For SGF 1 wt %-PET specimens, necking began at a strain of about 3%. Thus, deformation and failure proceeded in a ductile manner. Stress–strain curves for unreinforced PET specimens were similar to those for SGF 1 wt %-PET, except that the failure strain of the former was about 1300%. The SGF 30 wt %-PET specimens exhibited the maximum peak on the stress–strain curve and the final brittle-like catastrophic fracture occurred at a strain of about 5%. The SGF 60 wt %-PET specimens, on the contrary, were fractured in the process of increasing load in a brittle manner. The mechanical behaviour is influenced by microstructural parameters of fibre weight fraction and fibre length distribution as well as by failure characteristics in the composites. Another paper by the present authors [30] contains the results of studies on the effects of the microstructures and failure mechanisms on the mechanical behaviour.

3.2. Failure processes on the surface

Fig. 5 shows failure processes optically observed on the surface of an unreinforced PET specimen. As the load increased to a strain of about 3%, many tensile microcracks occurred and grew (arrow A). This microcracking may have resulted from inhomogeneities in the PET resin. Shear bands (arrow B) were formed at the sites of the microcracks. The growth direction of the shear bands was about 52° from the tensile direction. Friedrich et al. [1–4] and Schultz and Lhymn [5–8] have reported that crazing occurred in a semicrystalline PET modified by ionomeric particles. In the present case with non-modified PET specimens, however, the present authors have not yet found evidence that the described microcrackings were crazing. Enlarged SEM photographs suggest that they do not have a crazed structure. Therefore, the word "microcracking" is used in this article.

Failure processes on the surface of a SGF 1 wt %-PET specimen are shown in Fig. 6. Damage was hardly observable before loading (see Fig. 6a) but with an increase of load to a strain of about 1%, tensile microcracking and shear banding occurred in the matrix resin around the fibre ends. The tensile microcracking was caused by the tensile stress concentration at the fibre ends. The high interfacial shear strength between fibres and matrix must have affected the concentration [1]. With a further increase of the load to a strain of about 3% corresponding to the maximum stress level (see Fig. 6b and c), other tensile microcracks were formed in the matrix between fibres. These microcracks grew and were then bridged together by shear bands which had been formed at both tensile microcrack tips. Tensile cracks (arrow A) occurred following the microcrack growth. The shear bands grew into the matrix (arrow B) and were joined together by different shear bands. Although it is not clear in the picture, shear yielding proceeded along the fibre–matrix interface in the fibre length direction. Shear cracking followed this shear yielding, which caused the fibres to pull out of the matrix (arrow C). Some fibres were broken (arrow D), which induced other tensile microcracks and also shear bands in the

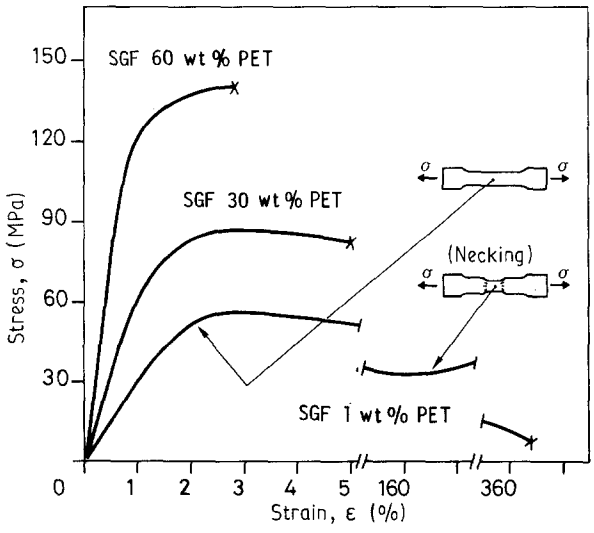

Figure 4 Stress–strain curves of SGFR-PET specimens.

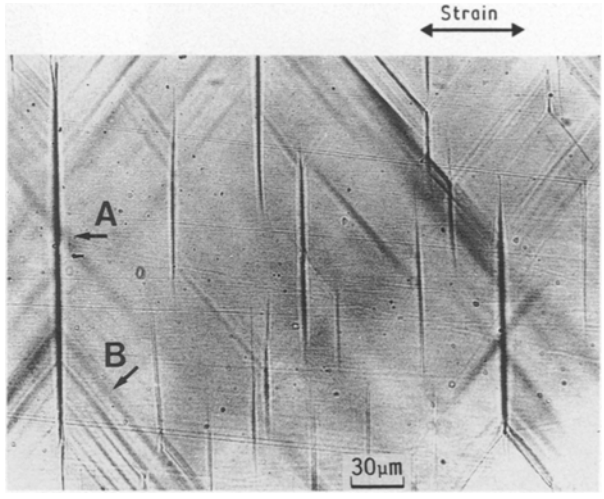

Figure 5 Polarized optical microscopic observation of failure processes on the surface of an unreinforced PET specimen.

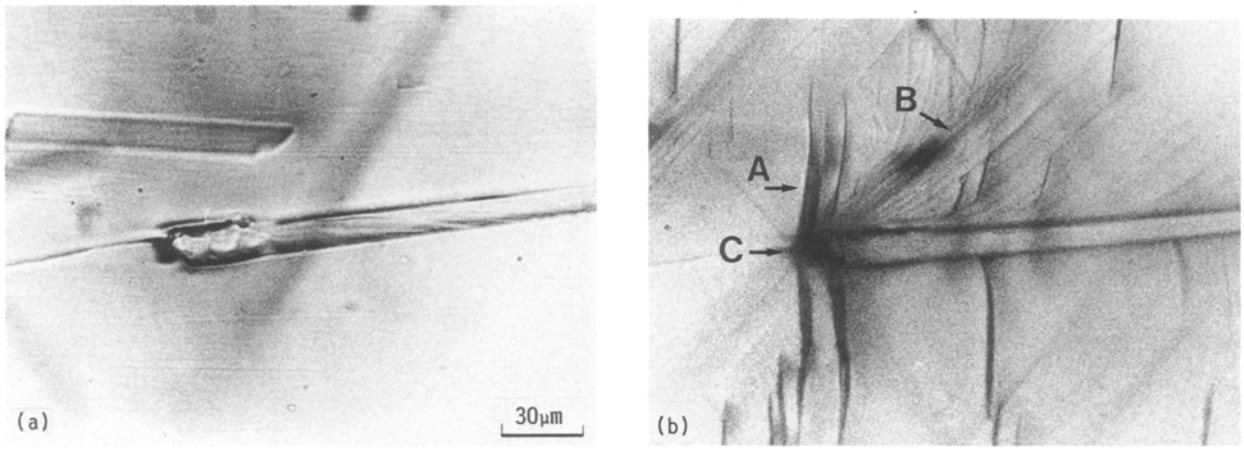

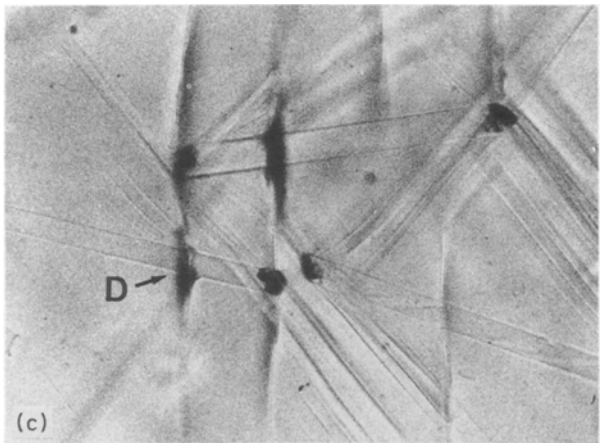

Figure 6 Polarized optical microscopic observation of failure processes on the surface of a SGF 1 wt %-PET specimen (a) before loading, (b) after loading to a strain of about 3%, and (c) same loading as (b) (~ 10 μm from surface).

matrix. The most important factors in the fracture processes above were considered to be the microcrack-induced tensile cracks at the fibre ends which grew into the matrix. These tensile cracks were very influential in the catastrophic fracture initiation on the specimen surface. The tensile cracks were formed up to about 15 μm in depth beneath the surface. The result was similar also with SGF 30 wt % and SGF 60 wt %-PET specimens. Based on the above observation, the failure mechanisms on the surface of SGF 1 wt %-PET are schematically presented in Fig. 7.

In situ SEM photographs were obtained to study the surface morphology of a SGF 30 wt %-PET specimen as shown in Fig. 8. Microcrack-induced tensile cracks occurred at the broken or unbroken fibre ends during loading to a strain of about 2.6% corresponding to the maximum stress level, and grew into the matrix (arrow A in Fig. 8a). Shear yielding took place around the fibre ends and was followed by shear cracking along the interface in the fibre length direction (arrow B). The shear crack induced voiding as well as fibre pull-out from the matrix at the fibre ends. The shear yielding and shear cracking along the interface may have proceeded in parallel with the shear band growth in the matrix (see Fig. 6b). With further loading, the tensile cracks and the shear cracks described above joined together (arrow C in Fig. 8b) to initiate a macroscopic fracture (see dotted line in the figure). Thus, both microcrack-induced tensile cracks and shear band-induced cracks were considered to have a cooperative effect on catastrophic fracture initiation. The failure mechanisms on the surface of SGF 30 wt %-PET specimens are schematically shown in Fig. 9.

Fig. 10 shows a typical SEM photograph taken of the surface of a SGF 60 wt %-PET specimen just before catastrophic fracture of the specimen. Growth of the tensile cracks at the fibre ends (arrow A) was suppressed by other closely neighbouring fibres. Instead, shear-mode failure proceeded in the matrix between fibres (arrow B). Shear cracks propagated on the matrix side near the interface (arrow C) like partial delamination. Sato *et al.* [17] observed the partial delamination which proceeded between broken fibre ends in unidirectional long-fibre reinforced plastics with a fibre concentration of 60 vol % under uniaxial tension. Shear stress interaction may have been greatly enhanced by the closeness between fibres and

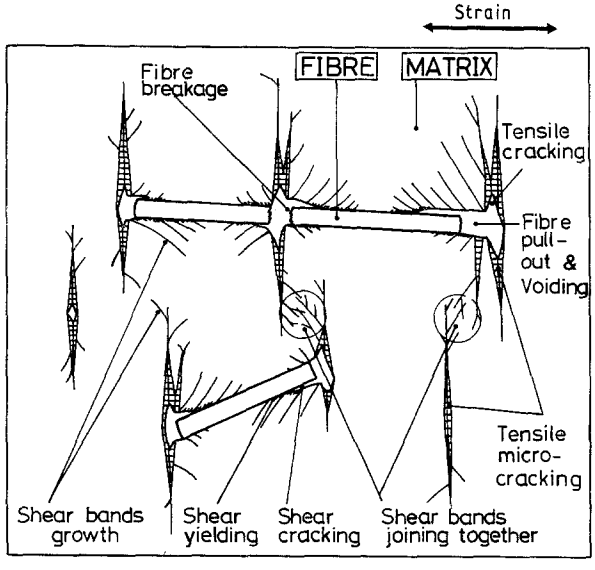

Figure 7 A schematic drawing of failure mechanisms on the surface of SGF 1 wt %-PET specimens.

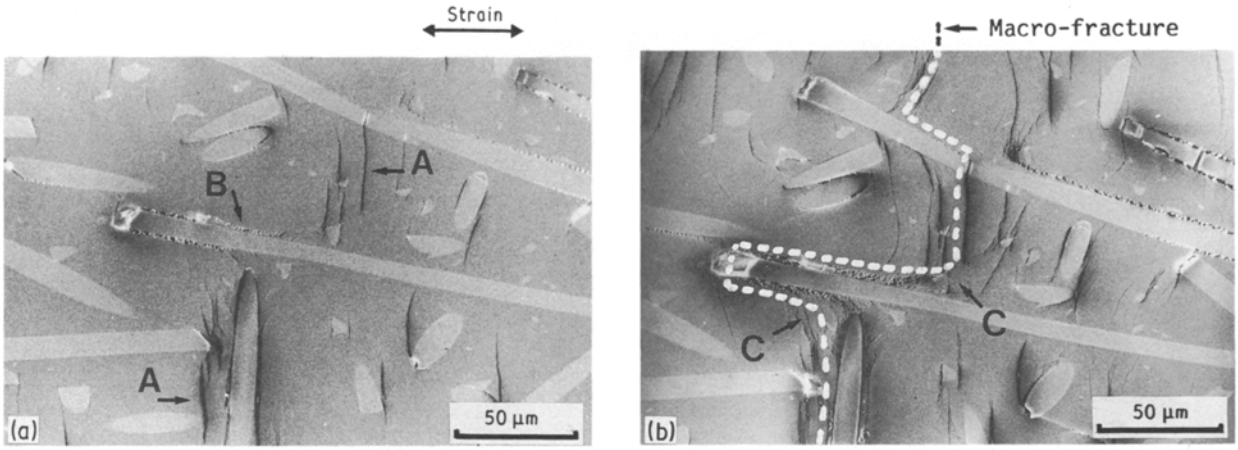

Figure 8 *In situ* scanning electron microscopic (SEM) observation of failure processes on the surface of a SGF 30 wt %-PET specimen (a) after loading to a strain of about 2.6%, and (b) just before catastrophic fracture.

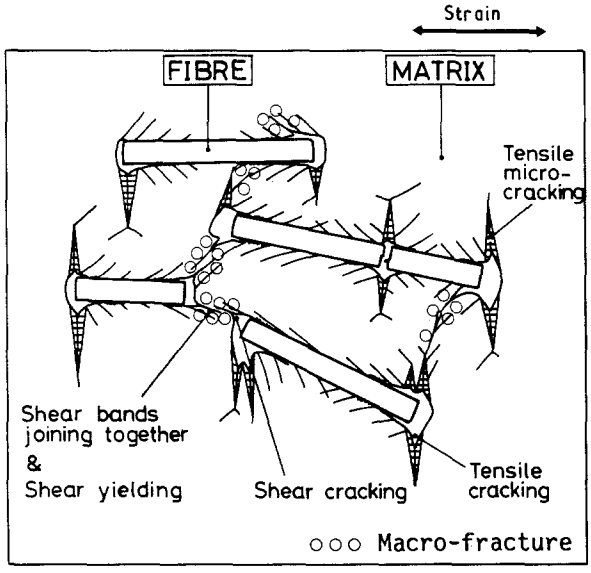

Figure 9 A schematic drawing of failure mechanisms on the surface of SGF 30 wt %-PET specimens.

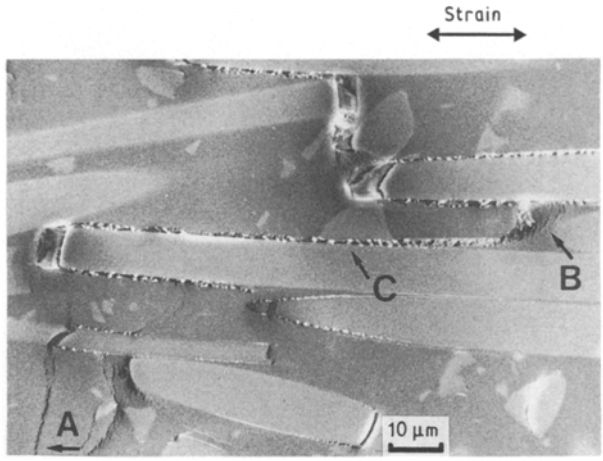

Figure 10 *In situ* SEM observation of failure processes just before catastrophic fracture of a SGF 60 wt %-PET specimen.

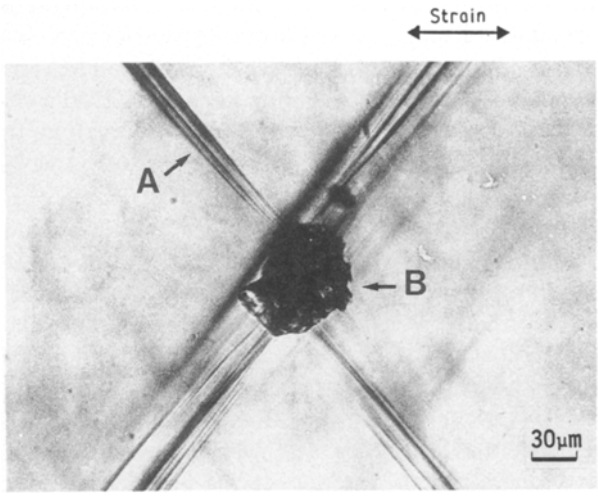

Figure 11 Polarized optical microscopic observation of failure processes in the interior of an unreinforced PET specimen.

also their orientation toward the tensile direction (see Fig. 2c) [9, 16, 21]. The enhanced interaction must have had an effect on the delamination-like failure. Thus, the shear cracks strongly influenced catastrophic fracture initiation on the surface of SGF 60 wt %-PET specimens.

3.3. Failure processes in the interior

Fig. 11 shows a polarized optical micrograph taken in the interior of an unreinforced specimen. During loading to a strain of about 3%, shear bands (arrow A) were observed at some probable inclusion sites (arrow B). The growth direction of these shear bands was almost the same as that on the surface. In addition, debonding took place along the interface between the inclusions and resin. No discernible tensile cracking occurred in this case. It is worth noting that the failure processes in the interior of unreinforced specimens were different from those on the surface (Fig. 5).

Failure processes in the interior of a SGF 1 wt %-PET specimen were also somewhat different from those on the surface. The polarized optical photographs in Fig. 12 were taken in the interior of the specimen in Fig. 6. Little damage was observed before loading (see Fig. 12a). Shear bands were formed with the increase of load around the fibre ends. Shear cracking occurred at the fibre ends as the shear bands

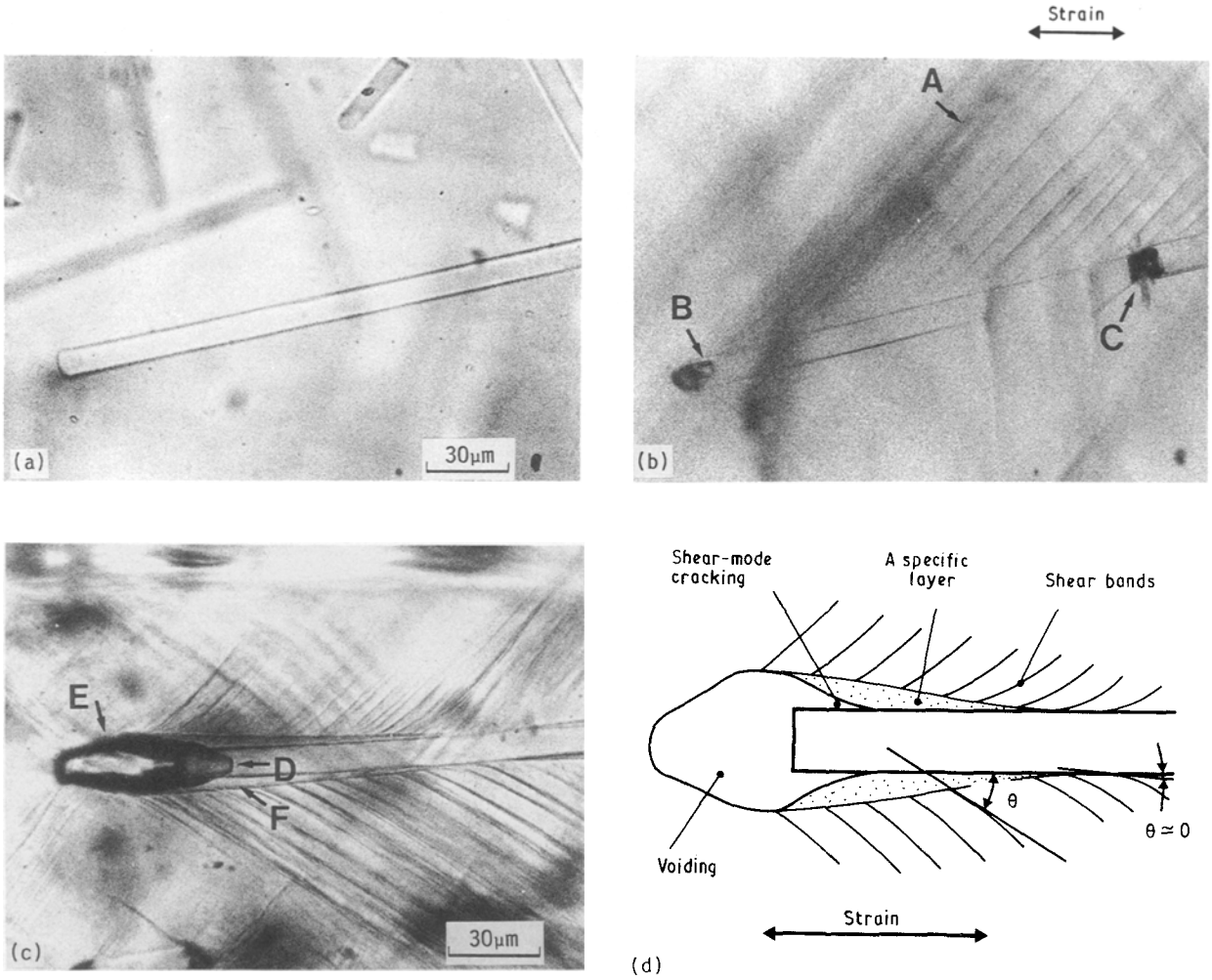

Figure 12 Polarized optical microscopic observation of failure processes in the interior of a SGF 1 wt %-PET specimen (a) before loading, (b) after loading to a strain of about 3%, (c) after loading to a strain of about 160%, and (d) a sketch from micrograph (c).

grew and proceeded on the matrix side near the interface. As the load increased further, to a strain of about 3%, the shear bands grew much more (arrow A in Fig. 12b) and joined with other shear bands. The shear cracks at the fibre end grew further in the fibre length direction (arrow B). Similar to the case of Fig. 6c, some fibres were broken (arrow C), causing tensile microcracking and shear banding around the broken ends. During loading to a strain of about 160%, the shear crack propagation (arrow D in Fig. 12c) induced pull-out of the fibres from the matrix as well as voiding at the fibre ends (arrow E). The voids grew into the matrix and joined together causing catastrophic fracture.

It should be noted that a "specific layer" appeared at the foot of the shear bands during the deformation (see arrow F in Fig. 12c). A sketch drawn based on the above failure process observed around the fibre end is shown in Fig. 12d. The angle, θ, between fibre length direction and shear banding direction at the foot of the bands increased considerably from almost zero at the initial stage as deformation increased around the fibre end. In order to check whether the layer was vacant or not, the morphology of the layer was examined optically as follows: Fig. 13 presents optical micrographs taken from the surface of the same polished thin specimen as shown in Fig. 12c. A fibre with the specific layer was observed under the transmitted and reflected light as shown in Fig. 13a and b, respectively. The fibre was not the same as the one in Fig. 12c, but a part of it had been exposed on the surface. Fig. 13c presents a schematic drawing based on the results of Fig. 13a and b. The specific layer adjacent to the exposed part of the fibre (arrows A and A′) was not vacant but contained matrix material. Very few macrovoids or discrete shear cracks were observed in the layer. These observations confirmed that the layer was not a shear crack. This type of layer has also been observed in specimens of SGF 30 wt % and 60 wt %-PET. Interfacial shear failure has been discussed by several authors. Friedrich [2] suggested the sequence of the shear crack formation in case of cohesive failure between fibres and matrix could be: (a) microcracking, (b) formation of shear crazes, (c) shear macrovoiding, and (d) shear fracture between the macrovoids. Lhymn [8] reported that discrete shear cracks were formed similar to the above processes (a) and (b), but that the cracks are connected by shear deformation. Thus, the fibre is pulled out with the residual matrix phase adhering to the fibre surface. The specific layer, on the other hand, was observed on the matrix side near the interface. This layer is thought to be a kind of plastic deformation layer which was transformed from severely deformed shear bands around the fibre end. It

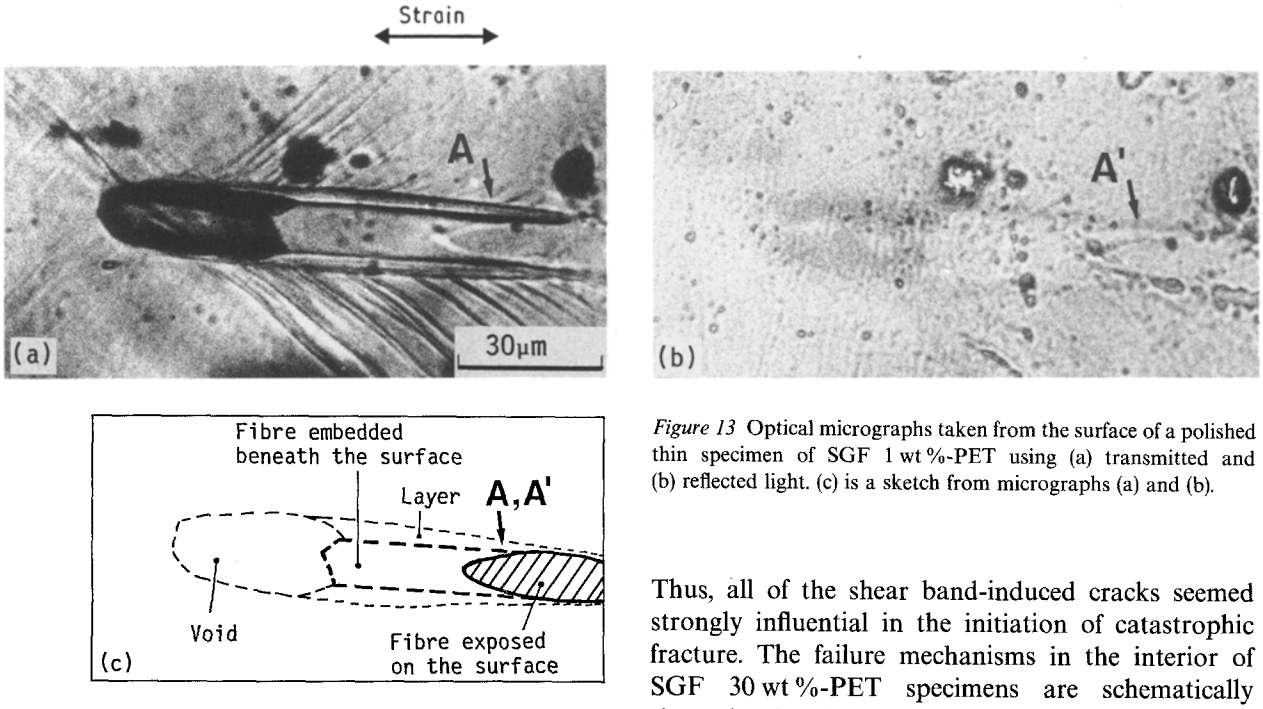

Figure 13 Optical micrographs taken from the surface of a polished thin specimen of SGF 1 wt %-PET using (a) transmitted and (b) reflected light. (c) is a sketch from micrographs (a) and (b).

is therefore considered to be a kind of transition layer from the shear bands to the shear cracks near the interface.

The above observed failure mechanisms in the interior of SGF 1 wt %-PET specimens are schematically presented in Fig. 14. The growth and joining-together of the shear band-induced voids at the fibre ends exhibited strong effects on the catastrophic fracture initiation, which was different from the failure processes (see Fig. 7) on the surface.

It is possible that the material state and residual stresses in the interior were somewhat different from those on the surface and that this circumstance caused the different failure processes. We examined the failure mechanisms in a similar way for specimens after polishing to a half, one third and one quarter of the original thickness. However, the results were the same as those for the unpolished as-moulded specimens. Specimens of SGF 30 wt % and SGF 60 wt %-PET also exhibited similar results. This suggests that change in the material state and the existence of residual stress had, little if any, effect on the occurrence of the different failure processes. It seems that the existence of different stress fields around each fibre, either on the surface or in the interior, caused the above results. This has been studied by finite element calculation [31].

Fig. 15 shows failure processes optically observed in the interior of a SGF 30 wt %-PET specimen. With an increase of load to a strain of about 2.6%, which corresponds to the maximum stress level, shear cracks (arrow A' in Fig. 15a) near the interface were propagated in the fibre length direction and the shear bands also grew around the fibre ends (arrow A). The specific layer was also observed to form in the matrix near the interface (arrow B). With further loading up to catastrophic fracture, the shear cracks induced matrix macrocracking (arrow C in Fig. 15b) and caused pull-out of the fibres from matrix (arrow D).

Thus, all of the shear band-induced cracks seemed strongly influential in the initiation of catastrophic fracture. The failure mechanisms in the interior of SGF 30 wt %-PET specimens are schematically shown in Fig. 16 and were also different from those on the surface (see Fig. 9), where tensile cracks at the fibre ends had an effect on the fracture initiation.

A polarized optical micrograph taken just before catastrophic fracture of a SGF 60 wt %-PET specimen is presented in Fig. 17. Delamination-like shear cracks near the interface were also recognized (arrow A in Fig. 17) indicating similar fracture processes to those on the surface (see Fig. 10). The shear cracking was also very important in the initiation of catastrophic fracture.

The interior failures have been believed to control the failure processes throughout the specimens, because the failures on the surface dominated only up to about 15 μm underneath the surface as stated in Section 3.2. This gives very useful insights for the investigation of the ultimate and/or failure strength of short-fibre reinforced composites. Further study of

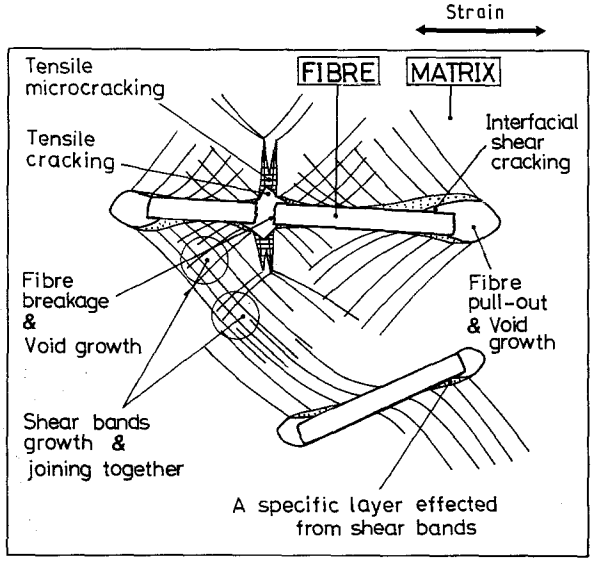

Figure 14 A schematic drawing of failure mechanisms in the interior of SGF 1 wt %-PET specimens.

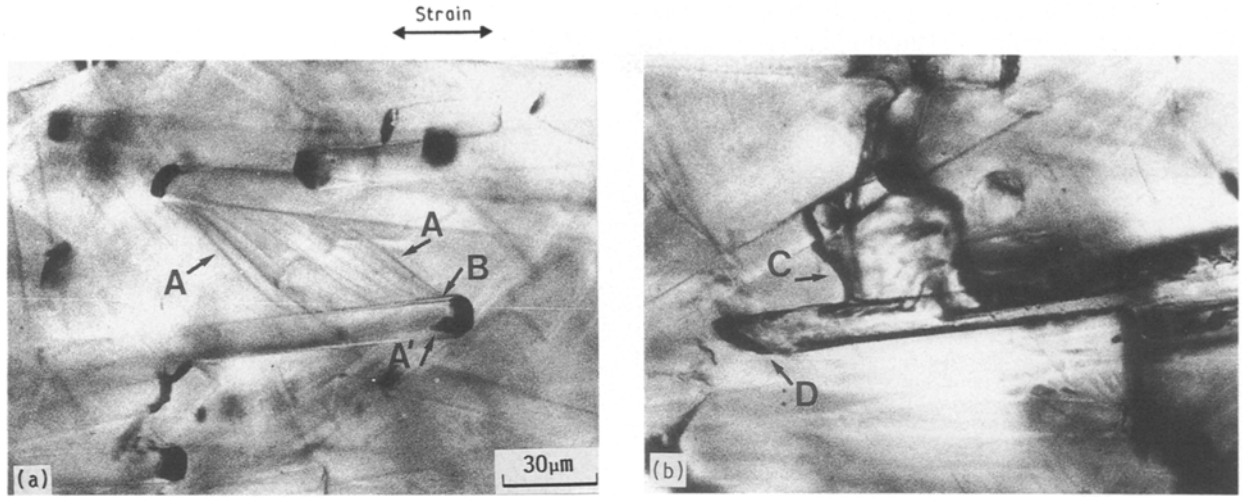

Figure 15 Polarized optical microscopic observation of failure processes in the interior of a SGF 30 wt %-PET specimen (a) after loading to a strain of about 2.6%, and (b) just before catastrophic fracture.

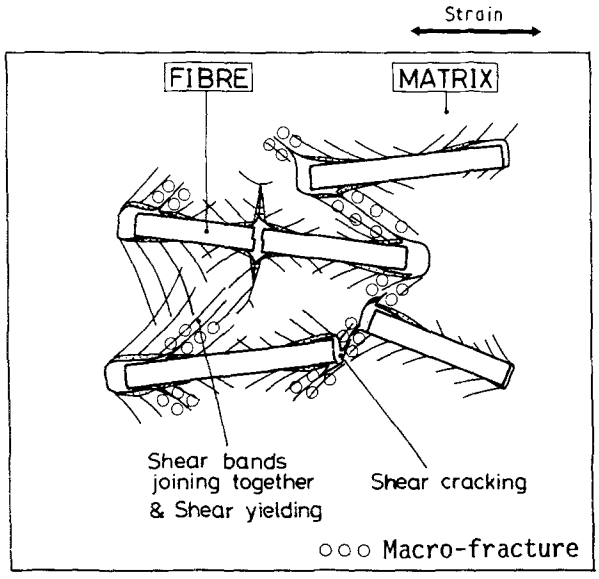

Figure 16 A schematic drawing of failure mechanisms in the interior of SGF 30 wt %-PET specimens.

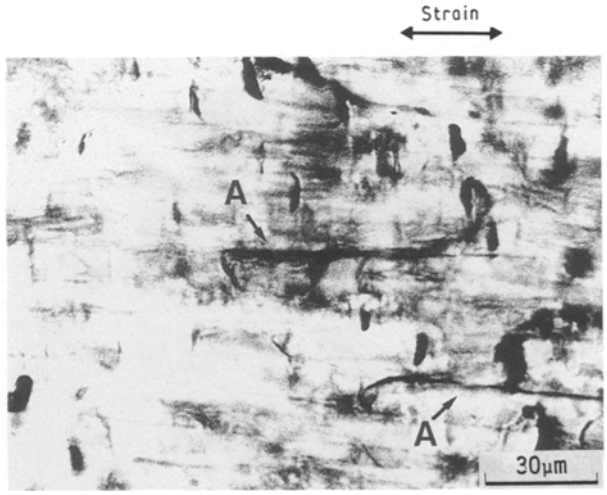

Figure 17 Polarized optical microscopic observation of failure processes in the interior of a SGF 60 wt %-PET specimen.

TABLE I Influential factors in catastrophic fracture initiation in unreinforced and short-fibre reinforced PET specimens.

wt%	Surface	Interior
Unreinforced PET	▲ Tensile microcracking	● Shear band formation
SGF 1 wt %-PET	▲ Tensile cracks growing at fibre ends	● Shear band-induced voids growing at fibre ends
SGF 30 wt %-PET	▲ Tensile cracks growing at fibre ends ● Shear crack propagation along fibre–matrix interface and/or between fibres	● Shear crack propagation along fibre–matrix interface and/or between fibres
SGF 60 wt %-PET	● Shear crack propagation along fibre–matrix interface and/or between fibres	

strengthening behaviour of the composites by using the interior failure mechanisms is introduced in another paper [30].

4. Conclusions

Table I summarizes the factors influencing catastrophic fracture initiation in unreinforced and short-glass-fibre reinforced PET specimens. The failure mechanisms on the specimen surface were different from those in the interior and were greatly affected by the fibre weight fractions. On the surface, tensile cracks growing at the fibre ends played a dominant role in the initiation and growth of catastrophic fracture. Their role became more important with decreasing fibre weight fraction. In the interior, on the other

hand, shear failure along the interface and/or between fibres was most influential in the initiation of catastrophic fracture for all fibre weight fractions. In conclusion, the shear failure in the interior almost controlled the failure processes throughout the specimens.

Acknowledgements

The authors are indebted to Dr A. Kato of Idemitsu Petrochemical Co. who kindly provided specimens for this study. They also appreciate the experimental assistance of Mr Y. Sakurada of their laboratory.

References

1. K. FRIEDRICH, in "Microstructure and fracture of fibre reinforced thermoplastic polyethylene terephthalate", Fortschr.-Ber. VDI-Zeitschr. Series 18 No. 12 (VDI-Verlag, Düsseldorf 1982).
2. *Idem*, in "Fracture Mechanical Behavior of Short Fibre Reinforced Thermoplastics", Fortschr.-Ber. VDI-Zeitschr. Series 18 No. 18 (VDI-Verlag, Düsseldorf 1984).
3. *Idem*, *Comp. Sci. Tech.* **22** (1985) 43.
4. J. KREY, K. FRIEDRICH and A. MOET, *Polymer* **29** (1988) 1433.
5. J. C. MALZAHN and J. M. SCHULTZ, *Comp. Sci. Tech.* **27** (1986) 253.
6. C. LHYMN and J. M. SCHULTZ, *J. Mater. Sci.* **18** (1983) 2029.
7. *Idem*, *Polym. Eng. Sci.* **24** (1984) 1064.
8. C. LHYMN, *J. Mater. Sci. Lett.* **4** (1985) 1323.
9. F. RAMSTEINER and R. THEYSOHN, *Comp. Sci. Tech.* **24** (1985) 231.
10. R. L. HOLLIS, R. HAMMER and M. Y. AL-JAROUDI, *J. Mater. Sci.* **19** (1984) 1897.
11. J. KARGER-KOCSIS and K. FRIEDRICH, *ibid.* **22** (1987) 947.
12. H. VOSS and R. WALTER, *J. Mater. Sci. Lett.* **4** (1985) 1174.
13. K. FRIEDRICH, K. SCHULTE, G. HORSTENKAMP and T. W. CHOU, *J. Mater. Sci.* **20** (1985) 3353.
14. R. W. LANG, J. A. MANSON and R. W. HERTZBERG, *ibid.* **22** (1987) 4015.
15. N. SATO, T. KURAUCHI, S. SATO and O. KAMIGAITO, *ibid.* **19** (1984) 1145.
16. *Idem*, *J. Comp. Mater.* **22** (1988) 850.
17. N. SATO, T. KURAUCHI and O. KAMIGAITO, *J. Mater. Sci.* **21** (1986) 1005.
18. P. T. CURTIS, M. G. BADER and J. E. BAILEY, *ibid.* **13** (1978) 377.
19. J. YUAN, A. HILTNER, E. BAER and D. RAHRIG, *ibid.* **20** (1985) 4377.
20. *Idem*, *Polym. Eng. Sci.* **24** (1984) 844.
21. T. F. MACLAUGHLIN, *J. Comp. Mater.* **2** (1968) 44.
22. W. H. BOWYER and M. G. BADER, *J. Mater. Sci.* **7** (1972) 1315.
23. F. RAMSTEINER, *Composites*, **12** (1981) 65.
24. K. STADE, *Polym. Eng. Sci.* **17** (1977) 50.
25. W-Y. CHIU and G-D. SHYU, *J. Appl. Polym. Sci.* **34** (1987) 1493.
26. B. FISA, *Polym. Composites*, **6** (1985) 232.
27. A. SALINAS and J. F. T. PITTMAN, *Polym. Eng. Sci.* **21** (1981) 23.
28. B. FRANZEN, C. KLASON, J. KUBAT and T. KITANO, *Composites*, **20** (1989) 65.
29. R. von TURKOVICH and L. ERWIN, *Polym. Eng. Sci.* **23** (1983) 743.
30. N. S. CHOI and K. TAKAHASHI, in "Proceedings of Benibana International Symposium on how to improve the toughness of polymers and composites" edited by I. Narisawa (Yamagata, Japan, 1990) p. 249.
31. N. S. CHOI and K. TAKAHASHI, *Comp. Sci. Tech.*, in press.

Received 5 March
and accepted 6 November 1990